Modelling of drying curves of silica nanofluid droplets dried in an acoustic levitator using the Reaction Engineering Approach (REA) model

Rosa Mondragón[1], J. Enrique Juliá[2,*], Leonor Hernández[2], Juan Carlos Jarque[1]

[1] Instituto de Tecnología Cerámica. Universitat Jaume I.

Campus de Riu Sec. 12071-Castellón de la Plana. Spain

[2] Departamento de Ingeniería Mecánica y Construcción. Universitat Jaume I

Campus de Riu Sec. 12071-Castellón de la Plana. Spain

* Corresponding author. E-mail: bolivar@emc.uji.es. Tel: +34 964728138. Fax: +34 964728106

Abstract

The use of nanoparticles has become of great interest in different industrial applications. The spray drying of nanofluids forms nanostructured grains preserving the nanoparticle properties. In this work, individual droplets of silica nanofluids were dried in an acoustic levitator. Tests were carried out under different experimental conditions to study the influence of the variables on the drying process. The drying curves were experimentally obtained and REA model was used to obtain the theoretical curves and the correlations for the activation energy. The critical moisture content theoretically obtained was used to predict the grain diameter.

Key words: Drying, kinetics, mass transfer, nanofluids, acoustic levitator

1 Introduction

In industry, spray drying is an essential unit operation for the production of granular powders with specific characteristics, granule size and moisture content, regardless of the dryer capacity and the product heat sensitivity. Spray drying is the transformation of a given feedstock from a fluid state into a dried particulate structure by spraying the feed into a hot drying medium. This causes the evaporation of the droplet solvent, leading to formation of particulates [1]. This process is used in the manufacture of many industrial products such as ceramics, food products, detergents and pharmaceuticals.

The drying behavior of a liquid-solid suspension droplet can be divided into two stages [1-3], whose kinetics are shown in Figure 1. In the first stage, the droplet containing large amount of liquid content enters the hot medium, undergoes sensible heating up to wet bulb temperature and then evaporation from the droplet surface starts (AB section) resulting in the droplet shrinking. The moisture migrates from the inner part of the droplet, rapidly enough to maintain surface saturation. As a consequence, the droplet surface is fully wetted and the liquid evaporates at the droplet surface. This stage is also known as the constant rate drying stage, since the change of droplet moisture per unit time remains steady (BC section). The diameter, d, decreases following the d^2-relation, and the maximum drying rate value is achieved. At the critical moisture content (point C), the entire droplet surface cannot longer be maintained saturated by moisture migration and the second drying period begins. In this period, called falling rate period, a shell is formed on the droplet surface and the evaporation occurs through the pores of that shell, with the vapor diffusing out to the surface (CE section). The drying rate decreases as the thickness of the shell increases. Two sub-sections can appear in this period depending on the material that is being dried (CD and DE sections). The drying process ends when the granule achieves the equilibrium moisture content with the surrounding medium.

In the drying process of a small droplet containing nanoparticles, just after the shell formation at the end of the first drying period, the liquid forms concave menisci between particles that produce attractive capillary forces between the shell particles, promoting the acceleration of that shell towards the droplet centre. Due to the liquid menisci on the outer shell surface, the shell undergoes compressive stress and shrinks leading the shell to submerge into the liquid [4, 5]. That liquid covers again the droplet surface and evaporates freely until its level is reduced to create menisci between particles. These menisci lead the shell to shrink again. As a result, a transition period between first and second drying stages appears. The process of evaporation in the transition period comprises series of surface evaporation and shell shrinking processes. When the shell strength becomes greater than the capillary forces, due to its thickness, the shell shrinking stops and the second drying period begins.

The main objective of the researchers in this field is to know the effect of the variables that influence the drying process on the final properties to be able to control it and therefore to produce granules of desired characteristics suitable for each application. In this way, the main parameters affecting the drying can be classified in operational conditions: inlet air temperature, relative humidity of the air, atomizing suspension feed rate and spray size distribution; and feed characteristics: initial solid mass load, primary particle size, viscosity, flocculation state and surface tension.

Drying models predicting the drying kinetics of single droplets can be used to relate the final powder properties (such as the final grain diameter, mean porosity, compacity, morphology, microstructure, etc.), with the spray dryer design and process parameters. Moreover, in recent years, the spray drying process has become a frequent subject for computational fluid dynamics (CFD) modeling [6, 7]. However, it is important to be able to correctly model the drying kinetics of the suspended droplets in order to predict the

performance of a spray dryer. If the drying model is inaccurate, the following predictions will also be inaccurate. All the information obtained from the drying of single droplets can be introduced in the CFD model to conduct simulations of industrial scale spray dryers. These simulations can be used to study and control the behavior of the spray dryers and the drying process to improve the process efficiency and the quality of the final product.

The drying models available can be classified in three different categories [3, 8-10]:

1. Models that solve simultaneously the continuity, momentum, energy, and species conservation differential equations using the diffusion equations and coefficients [4, 5, 11-19]. The solution of these set of equations is complicated by the presence of a moving domain boundary because of the shrinking droplet radius in the first drying stage and the receding interface between the dry crust and wet core regions of the wet particle in the second drying stage. The numerical solution of such models is a complex problem and demands significant computer resources and time. In addition, these models usually require knowledge of many coefficients like thermal and mass diffusivities, particle porosity, critical moisture content, etc., under different moisture and temperature conditions.

2. Models based on a semi-empirical approach that utilizes the concept of characteristic drying curve (CDC) [9, 13, 20-22]. In this model the first drying stage is simplified by analogy with the evaporation of a small pure liquid droplet. For the falling rate period, the drying rate in a CDC model is determined by the drying rate at the end of the first drying stage multiplied by a function depending on critical, equilibrium, and current moisture content values. The model is simple and does not require high mathematical efforts. However, it is necessary to know a priori the critical moisture content that depends on the drying conditions. The model is suitable for materials in which the first dying period does

not exist or is very short. In this case the critical humidity can be replaced by the initial moisture content.

3. Drying models based on reaction engineering approach (REA) [8-10, 16, 22-26]. The main theory of the model considers the drying as an activation process in which an energy barrier has to be overcome for moisture removal to occur. In the mathematical expression of the model, the vapor concentration gradient is considered the driving force for the drying. The water removal process is represented by an activation energy which value is zero when the solid is fully covered by water, and increases as the moisture content decreases, due to the difficult of water removal for low contents. Authors have found this model promising due to its simplicity and high accuracy at different drying conditions. However, the model applicability is limited by the range of materials whose drying behavior has already been experimentally studied (skim milk, whole milk, lactose, proteins, sucrose, maltodextrin…). The reason is that the model uses a correlation for the activation energy that depends on the material and drying conditions, and has to be determined experimentally.

All the previously mentioned models have to be checked with experimental data obtained from the drying process of single droplets. In all the previous works mentioned above the experimental data were obtained drying single droplets by means of the glass filament method. This method has the disadvantage that the droplet is in contact with the filament and it is not completely isolated. In the last decade acoustic levitators has been extensively used to study the drying behavior of pure liquids, multi-component liquids and liquid–solid suspension droplets [2, 27-37]. The use of levitators has allowed measuring the droplet shape, the evaporation rates in both drying periods and the humidity curves. Levitator tubes (acoustic, optical, electrodynamic and aerodynamic types) exhibit some advantages over conventional methods, since there is no mechanical contact with the droplet. The

experimental complexity of the ultrasonic levitators is less than the aerodynamic ones and allows working with almost any liquid over a wide range of diameters of droplets (from 0.1 mm to several mm). In contrast to the other levitation techniques, acoustic levitation has the advantage of not requiring any specific physical properties (e.g. a certain electric charge or refractive index) of the sample. Moreover, acoustic levitation provides stable sample position, easy access to the sample and low costs for supply and operation [38].

In this work single droplets of silica-water nanofluids were dried in an acoustic levitator under different experimental conditions of initial solid mass load, Y_S, *pH* value, salt concentration, *[NaCl]*, air temperature, T, and initial droplet volume, V_0. The ANOVA method was used to analyze the effect of the input variables on the first period transfer rate. The drying curves (X=f(t)) were experimentally obtained for each conducted test and the REA model was used to model the experimental data. To do this, correlations for the activation energy were obtained for this system at different drying conditions. Moreover, the parameters obtained for each measured test were found to depend on the solid content and the drying temperature and were fitted to a multiparametric equation. These correlations enlarge the existing database which only contains activation energies for materials used in the food industry.

2 Experimental set-up and measurement techniques

The experimental set-up is composed of three systems (Figure 2 a) [32]:

- An acoustic levitator consisting of an ultrasonic 58 kHz horn and a concave reflector (tec5 AG Sensorik und Systemtechnik). The levitator was modified in order to work at high temperature conditions up to 150ºC. Two separated metallic chambers can be found in the levitator tube (Figure 2 b). The section identified as “cold chamber” contains the ultrasonic transducer of the levitator. The temperature is controlled by

forced convection using cold air flow. The second section is identified as “hot chamber”, and contains the lower part of the levitator, the reflector and the multiphase droplet. The temperature of this chamber is controlled by an electric heater at the wall and an air stream that enters the levitator tube through an array of holes located in the reflector.

- An optical system consisting of a white light source with a diffuser and a CMOS camera with a macro lens. The CMOS camera (UI-1220M, IDS-Imaging Development Systems GMBH) (752x480 pixels, 87 frames per second) and the back-light illumination system are used to measure the droplet cross-sectional area and the vertical position of the droplet during the drying process.
- A gas conditioning system (not shown in the figure) controls the temperature, flow rate and relative humidity of the air inside the levitator tube. The air conditioning system (CEM System W-202A, Bronkhorst High-Tech B.V) is composed of an air-drying cartridge, a two-mass flow controllers and a mixer/evaporation unit. This system allows temperatures up to 200ºC and a humidity up to a dew point of T=80ºC. The flow rate of the air stream was set to 0.5 l/min and it was used to ensure constant drying conditions around the droplet and to ventilate the acoustically induced vortex system around the droplet from liquid vapor.

The experimental set-up allows the selection and control of the input parameters and also the recording of the drying process of the droplet within the levitator tube. The images were processed with Matlab, so that the equivalent diameter and the position of the droplet during the drying process could be obtained. This information was used to calculate the mass transfer rate of the two drying periods and the moisture content at each time of the process.

In order to calculate the mass transfer rates, equations 1 to 3 were derived from the work by Kastner et al. [30]. The instantaneous mass transfer rate for the first drying period

($m_{L,1}$) is calculated by the decrease of the droplet volume. This mass transfer rate is defined as,

$$m_{L,1} = -\frac{\pi}{6}\rho_L \frac{d_1^3 - d_2^3}{t_1 - t_2} \tag{1}$$

where ρ_L is the liquid density, d is the droplet diameter and the sub-indexes 1 and 2 denote two consecutive instants during the drying process.

The mass transfer rate of the second drying period ($m_{L,2}$) is calculated using the position of the droplet inside the acoustic field. If this position is assumed to be dependent on the droplet density, the mass transfer rate during this period can be calculated as,

$$m_{L,2} = \frac{M_{21}}{t - t_{21}} \frac{y(t) - y_{21}}{y_{22} - y_{21}} \tag{2}$$

where y_{21} and y_{22} are the droplet positions at the beginning and the end of the second drying period respectively, $y(t)$ is the instantaneous position of the droplet, and M_{21} is the liquid mass content in the droplet at the end of the first drying period previous to the shell formation. It is calculated as the difference between the initial water content and the total evaporated water at this moment,

$$M_{21} = \frac{\pi}{6} d_0^3 \rho_{Sus} (1 - Y_S) - \frac{\pi}{6}\rho_L (d_0^3 - d_f^3) \tag{3}$$

where d_0 is the initial droplet diameter, d_f represents the droplet diameter at the end of the first drying period or final grain diameter, Y_S the initial solid mass load in the suspension and ρ_{Sus} is the density of the suspension, which in turn can be evaluated as,

$$\frac{1}{\rho_{Sus}} = \frac{Y_S}{\rho_S} + \frac{(1 - Y_S)}{\rho_L} \tag{4}$$

where ρ_S is the density of the solid particles in the suspension.

With the initial water content and the liquid evaporation rates, the quantity of water present in the droplet/grain at each moment, can be easily calculated. The dry basis moisture, X, is defined as the ratio between the water and solid contents:

$$X = \frac{M_L(t)}{M_S} \tag{5}$$

where M_L is the mass of water and M_S is the mass of solid present in the droplet, which remains constant during all the drying process:

$$M_S = \frac{\pi}{6} d_0^3 \rho_{Sus} Y_S \tag{6}$$

3 Suspensions and experimental matrix

All the experiments were carried out with silica-water nanofluids. In this work, commercial fumed silica provided by Degussa was used. The silica chosen was Aerosil 200, which consists of amorphous hydrophilic silica nanoparticles with primary units of 12 nm and density of 2200 kg/m^3 according to the manufacturer. Nanofluids with different particle concentrations were prepared by adding distilled water to the defined amounts of nanoparticles. In this method, known as the two-step method, the nanoparticles are purchased in dry powder and then dispersed in the liquid medium. The dispersion was made using an ultrasonic probe (UP400s from Hielscher Company) that has been checked to be the most effective dispersion system [39]. Initially, the mixture of nanoparticles with the water was submitted to a sonication treatment for 3 minutes. Afterwards, the *pH* of the nanofluid was modified by adding HCl or NaOH solutions (0.01 w/w). Finally, to ensure a correct dispersion of all the components, the nanofluids were submitted to a second sonication treatment during 2 minutes. For this material the isoelectric point (IEP) was experimentally determined from the zeta potential curves and a *pH*=2 value was obtained.

In order to gather the process experimental data and the drying kinetics at different experimental conditions a Design of Experiments (DoE) was planned. In this case, a matrix based in a fractional factorial design, 2^{k-1}, was performed. Five variables including solid mass load (0.02 w/w < Y_S < 0.20 w/w), *pH* of nanofluids (2 < *pH* < 10), salt concentration (0 M < *[NaCl]* < 0.05 M), ambient air temperature (80ºC < *T* < 120ºC) and initial droplet volume (0.3 µl < V_0 < 0.8 µl) were chosen to study their effect on the drying kinetics. A total number of 16 tests were carried out for the five input variables. Moreover, drying tests at Y_S = 0.10 were carried out to obtain correlations for the required parameters in the activation energy equation. The experimental correlation obtained was used to predict the drying curve of droplets dried at *T* = 100ºC and to check its applicability. Each test was repeated from six to eight times in order to evaluate the reproducibility of the experimental set-up and to obtain a mean value for the drying kinetics.

4 Results and discussion

4.1 Drying behavior

For each of the measured experiments, the evolution of the squared-diameter and the position of the droplet were measured. From these curves the existence of the different drying periods as well as the buckling phenomenon can be analyzed. All the experimental tests present a first drying period, at constant rate, followed by a second drying period. The transition period, in which the shell shrinks and the buckling takes place, depends on the *pH* value and the interparticle forces present in the nanofluid. Figure 3 shows the obtained curves for two different drying conditions in which the vertical lines indicate the limits among the first drying period, the transition period and the second drying period. The shape of the droplet at different times is also shown. During the first drying period, particles move towards the inner part of the droplet to minimize its surface energy [40]. The surface energy

of the liquid-vapour interface is lower than that of the solid-vapour one and so the particles move, thus allowing the droplet surface to be completely wetted and the liquid to evaporate at the droplet surface. The droplet shrinks progressively while preserving the spherical shape. The onset of buckling takes place when the surface can not be kept saturated by moisture migration and particles collapse forming an elastic shell. The liquid that forms concave menisci between particles produce attractive capillary forces between them, promoting the acceleration of the shell towards the droplet centre. As result, the shell undergoes compressive stress and shrinks leading the shell to submerge into the liquid. The liquid is freely removed once again and the droplet diameter decreases continuously. It can be seen that a longer and more important transition period appears at the conditions of Figure 3 a). In this case the nanofluid is electrostatically stabilized (pH = 10) and the repulsion forces are important. When the first drying period ends and the shell is formed, the capillary forces that maintain the particles together have to overcome the electrostatic ones and the buckling process and the transition period are enhanced. The final shape of the grain is more irregular in this case as can be observed in Figure 3a). However, in Figure 3 b) (pH = 2, IEP) when the shell is formed, capillary and Van der Waals attractive forces lead the particles to aggregate and the droplet shrinks isotropically being the buckling process less significant. In this case the final grain is more spherical. The shrinkage of the shell ends when its strength becomes higher than the capillary forces. At this point starts the second drying period in which the grain diameter remains constant while the shell thickness increases due to the continuous incorporation of particles to the shell. Further removal of water takes place through the pores of the shell, increasing the difficulty of water diffusion as the shell thickness increases. This is the reason because the mass transfer rate decreases continuously and the drying process becomes slower in this stage.

Regarding the position of the droplet, levitation of a single droplet occurs because the acoustic force is counteracting the gravity force, allowing a fixed position of the droplet within the levitator tube during its drying process. Both the volume and the density of the droplet have an effect on the vertical position relative to the adjacent pressure node. However, it has been observed that the density change affects the droplet position more strongly that the change in volume [30]. During the first drying period and shrinking periods, the decrease of the squared droplet diameter is almost linear and the decrease of volume together with the loss of mass leads to an almost constant density that results in a stable droplet position inside the resonator. During the second drying period the droplet diameter is constant; however the droplet position inside the resonator varies. The variation of the droplet position is due to the change in the droplet density and mass. The volume remains constant, but the mass of the liquid, and therefore the mass of the grain, decreases because of evaporation.

After the drying process, dried grains were analyzed by SEM (Scattering Electron Microscopy). Images of the internal and external structure were taken. In Figure 3 micrographs are shown. All the drying conditions analyzed in this work produced hollow grains with shell formation. The degree of hollowness depends on the ability of the particles to rearrange and to diffuse inside the droplet during the first drying period [41-44]. The diffusivity of the particles depends mainly on the viscosity of the suspension which depends on the particle size. In this case, nanoparticles result in high viscosity suspensions and low diffusion coefficients compared to microparticle suspensions at the same solid content. If the particles can not diffuse easily, the collapse of the particles and the shell formation take place earlier in the drying process. As a result the final grain diameter is bigger and grains are hollower.

In all the experimental test cases in which the nanoparticles were dispersed in a salt solution in presence of NaCl, images show that salt crystals only appear at the grain surface, never in the inner part. In the drying process of droplets, during the second drying period, the position of the evaporation front depends on the operational conditions. As a consequence the diffusion of water through the pores of the shell can take place in liquid or in vapor phase. Inside the levitator, the acoustic stream provides a slower drying than in a spray drier and therefore under the experimental conditions analyzed in this work, the evaporation front is on the grain surface. That means that the liquid has enough time to diffuse through the particles and evaporates at the surface where the crystallization of the salt takes place. Size and shape of the crystals depends on the temperature and drying conditions. In Figure 4 images of the internal structure and the surface of several grains obtained under different experimental conditions in presence of NaCl are shown, so that the crystallization at the grain surface can be observed.

4.2 Mass transfer coefficients

Before modeling the drying behavior of droplets, the mass transfer coefficients, h_m, must be determined. In the drying of droplets acoustically levitated the acoustic field results in an acoustic stream that provides a drying mechanism stronger than the natural convection and dominates the process [45]. As a consequence, the available correlation provided by Ranz and Marshall in 1952 [46, 47] for the Sherwood number cannot be used:

$$Sh = 2 + 0.6\ \mathrm{Re}^{1/2}\ Sc^{1/3} \tag{7}$$

where *Re* is the Reynolds number and *Sc* is the Schmidt number.

Yarin et al., (1999) [34] developed a correlation for the Sherwood number that takes into account the acoustic boundary layer surrounding a levitated droplet. However, in this correlation the parameters that characterized the acoustic stream must be known or estimated:

sound pressure level, effective pressure amplitude of the incident acoustic field and angular frequency of the incident sound wave. Moreover, there is a parameter in the equation that changes as the droplet evaporates and must be re-calculated continuously.

In this work, the mass transfer coefficients were experimentally estimated in an easy way, so the values obtained can be applied directly to the drying of suspension droplets under the same experimental conditions. As can be seen, this coefficient depends on the Reynolds and Schmidt numbers which in turns depend on the temperature and droplet volume. Therefore, for each combination of air temperature and droplet volume, the mass transfer coefficient was obtained from the drying of pure liquid droplets by means of the mass conservation equation as follows:

$$\frac{dm_L}{dt} = h_m A \left[\rho_{v,d} - \rho_{v,a}\right] \tag{8}$$

$$\rho_L \frac{dV}{dt} = h_m A \left[\rho_{v,d} - \rho_{v,a}\right] \tag{9}$$

where $\frac{dV}{dt} = \frac{\pi d^2}{2}\left(\frac{d(d)}{dt}\right)$ and $A = \pi\ d^2$.

Equation 9 can be simplified to obtain a differential equation easy to integrate:

$$d(d) = \frac{2\ h_m \left[\rho_{v,d} - \rho_{v,a}\right]}{\rho_L}\ dt \tag{10}$$

$$d = d_0 + \frac{2\ h_m \left[\rho_{v,d} - \rho_{v,a}\right]}{\rho_L}\ t \tag{11}$$

where $\rho_{v,d}$ is the vapor density at the droplet surface (equal to the saturation vapor concentration for a pure liquid) and $\rho_{v,a}$ is the vapor density in the drying air.

The Sherwood number for the levitator can be calculated with the following equation:

$$Sh = \frac{h_m \, d}{D_{v,a}} \tag{12}$$

where $D_{v,a}$ is the diffusion coefficient of water vapor in the air

Figure 5 shows the evolution of the diameter during the drying of pure liquid droplets under the six combinations of air temperature and droplet volume analyzed in this work. Mass transfer coefficients were obtained by fitting the curves to Equation 11. The corresponding Sherwood numbers were calculated using Equation 12. In Table 1 experimental values and those obtained from equation 7 are shown. It can be seen that the acoustic stream provides a drying process slower than predicted by Ranz and Marshall for natural convection. In the literature revision values of the Sherwood number ranging from 2.5 to 8 were found for droplets dried in an acoustic levitator using the theoretical correlations, depending on the drying conditions of air temperature and droplet volume [34, 48]. In these previous works bigger droplets (V_0 = 1-3 μl) were dried at room temperature (T = 23 ºC). It can be also observed also in Table 1 that the Sherwood number increases as the droplet volume increases and the drying temperature decreases. Hence, Sherwood numbers higher than in this work were found because of these conditions.

4.3 Analysis ANOVA for the first period mass transfer rate

The results obtained for the first period mass transfer rate using Equation 1 were analyzed by means of ANOVA method, in order to establish the influence of the input variables on the first drying stage.

In the Pareto chart, the most sensitive input variables can be identified. This graph shows an ordered bar chart of the absolute effects scaled by P-values, essentially the number of standardized effects beyond the mean response. The line at 2.31 P-value represents a

significant level for achieving 95% confidence that a given effect did not just occur by chance.

Figure 6 a) shows the Pareto chart for the mass transfer rate where only the single effects were included. Any cross effect results of significance for the mass transfer rate in the analysis. Figure 6 b) shows the variation of the mass transfer rate when input variables change from the lower to the upper level. It can be seen that the input variables with higher influence in the first period mass transfer rate were the air temperature, the initial droplet volume and the solid mass load. All of them have a positive effect, meaning that an increase in their values leads to an increase in the mass transfer rate for the first drying period.

The drying of droplets is process controlled by heat and mass transfer. When a droplet gets in contact with a hot medium, there is transference of heat from the hot air to the droplet. This heat energy is transformed in latent heat at the droplet surface and it is used to evaporate the water. Then the water vapor is diffused from the droplet to the surrounding air. As a result, the driving forces for the drying process to take place are the gradients of temperature and moisture content between the droplet and the drying air. As expected, an increase in the drying air temperature leads to a higher temperature gradient between the heat carrier and the droplet surface, increasing the driving force for the drying to take place. As a result, the mass transfer rate in the first drying period increases.

The mass transfer rate also increases when increasing the initial droplet volume. The mass transfer rate is proportional to the mass transfer coefficient as can be seen in equation 8. The mass transfer coefficient is related to the Sherwood number (equation 12), which in turns, is proportional to the Reynolds number (equation 7). From the equations mentioned before, it is expected that an increase in the droplet volume, which leads to an increase in the Reynolds number produces a higher mass transfer coefficient between the droplet and the surrounding air. As a result, the mass transfer rate increases.

4.4 Application of REA model

The drying rate of a droplet can be expressed by means of Equation 8. However, for liquid-solid droplets, the vapor density at the solid-gas interface, $\rho_{v,d}$, is an unknown parameter which is time-dependent during the drying process. This parameter is related to the saturation vapor concentration, $\rho_{v,sat}$, (evaluated at the droplet temperature, T_d) by means of the relative humidity at the interface, φ_{surf}. This relative humidity can be expressed in terms of the activation energy needed for the drying process to take place:

$$\rho_{v,d} = \rho_{v,sat}(T_d)\ \varphi_{surf} = \rho_{v,sat}(T_d)\ \exp\left(-\frac{\Delta E_V}{R\ T_d}\right) \tag{13}$$

ΔE_v is expected to decrease to zero when liquid water fully covers the solid (making φ_{surf}=1) and increase to larger values when the average water content becomes small.

From Equations 8 and 13 the evolution of the moisture content can be obtained by means of the following equation:

$$\frac{dX}{dt} = -\frac{h_m\ A}{M_S}\left[\rho_{v,sat}\ \exp\left(-\frac{\Delta E_V}{R\ T_d}\right) - \rho_{v,a}\right] \tag{14}$$

where X is the dry basis moisture content, A is the droplet area and R is the gas constant.

The temperature of the droplet can be considered uniform through the droplet for Biot numbers less than 0.1 [10]. In this work, the value of this parameter is less than 0.07 for all tests and therefore, the droplet temperature could be considered uniform. The evolution of the droplet temperature was calculated by means of the energy balance equation with the help of the experimental data obtained for the drying curves.

$$m_d\ C_{p,d}\ \frac{dT_d}{dt} = h_C\ \ A\left(T - T_d\right) + \Delta H_v\ \frac{dm_L}{dt} \tag{15}$$

were m_d is the overall mass of the droplet, $C_{p,d}$ is the specific heat capacity of the droplet, h_C is the heat transfer coefficient, ΔH_v is the latent heat of water evaporation and dm_d/dt is the change of liquid content inside the droplet during the drying process.

In Figure 7 the evolution of the droplet temperature during the drying process is plotted together with the corresponding drying curve for one of the tests carried out. It can be observed that during the first drying period the droplet temperature remains constant and equal to the wet bulb temperature. During the second drying period the droplet temperature increases up to the drying air temperature.

The activation energy, which depends on the material and the drying conditions, was fitted to the expression:

$$\Delta E_V = a \exp\left[-b\,(X - X_{eq})^c\right] \tag{16}$$

where parameter a is constant, while parameters b and c depend on the solid content and the air temperature. The activation energy means the energy that must be applied to the droplet for the drying process to take place. Hence, the drying temperature and the moisture content, which are the driving forces of the process, must influence the activation energy [8].

From the evolution of the squared-diameter and the droplet position, the drying curves were obtained for each tested experimental condition. For the first drying period and intervals of diameter variation, Equation 1 was used to obtain the mass transfer rate. For the second drying period and intervals of constant diameter, the mass transfer rate was obtained from the evolution of position by means of Equation 2. With the initial moisture content and the water evaporation along the process, the droplet/grain moisture content was obtained by means of Equation 5.

Figure 8 shows the experimental data for the drying curves and the theoretical curves obtained by means of REA model. If Figures 8 a-d are compared, it can be observed that

when the drying temperature increases, the mass transfer rate also increases (as explained in section 4.3) and the drying time is shorter. It can be also concluded that the drying time is longer for bigger droplets due to the higher amount of liquid that has to be removed. The same situation can be found for lower solid contents in which higher amount of water has to be removed, being the drying time longer.

To model the drying curves, the mass transfer coefficients experimentally estimated for the drying of droplets in the acoustic levitator were used. For each experimental condition, the value of parameter *b* that provides the best fitting is shown in the figure. It can be seen that for low solid contents the parameter is independent on the temperature while for high solid contents, it increases when the temperature decreases. Table 2 shows the final mean values of all the parameters used in Equation 16 for each experimental condition. It can be seen that parameter *c* only depends on the solid content. In Table 3, the parameters obtained for the activation energy of different materials dried under different experimental conditions are shown so they can be compared with those found for silica nanofluids in this work. It can be observed that, even for similar operational conditions, the parameters depend mainly on the material being dried. The drying behavior depends not only on the operational conditions but also on the suspension conditions. Therefore the characteristics of the solid (particle size, particles size distribution and shape) influence the viscosity of the suspension and the packing of the particles, and then the drying behavior.

In the present study, for the silica system, empirical correlations were obtained to relate parameters *b* and *c* to the solid content and drying temperature. For the parameter *b*, a multiparametric fitting was done with all the values obtained in each individual test (20 data) and the following equation was obtained:

$$b = 1{,}217 + 29.193\ Y_S + 9.233 \cdot 10^{-3}\ T - 0.250\ Y_S\ T \qquad R^2 = 0.912 \qquad (17)$$

For the parameter c, a power fitting was done to relate the parameter to the solid content:

$$c = 0.735 - 1.178 \cdot 10^{-3}\, Y_S^{-1.582} \qquad R^2 = 0.999 \qquad (18)$$

In order to check the applicability of the correlations obtained, the parameters for Y_S = 0.10 and T = 100ºC were obtained. The resulting values were b = 2.56 and c = 0.69. With this information the drying curves for Y_S = 0.10, T = 100ºC, V_0 = 0.3 – 0.8 µl, pH = 10 and $[NaCl]$ = 0 M were predicted. The calculated curves were compared with the experimental values obtained from tests carried out under these conditions. In Figure 9 the good agreement between experimental and theoretical curves can be seen.

Finally, the final grain diameter can be related with the critical moisture content by means of the following equation [16]:

$$d_f = d_{cr} = d_0 \sqrt[3]{\frac{\rho_L + X_{cr}\,\rho_S}{\rho_L + X_0\,\rho_S}} \qquad (19)$$

From the theoretical curves, the critical moisture content can be obtained. This moisture content corresponds to the value at which the transition from first to second period takes place, at the point in which a change in the slope of the curves occurs. For each experiment, the critical moisture content was obtained experimentally and theoretically from the drying curves. In Figure 10 it can be seen that the theoretical results show a good agreement with the experimental ones.

The theoretical final grain diameter was obtained using the theoretical moisture content and Equation 19. The obtained results were compared with those derived from the image processing of the videos recorded for each experimental test. Figure 11 shows a good agreement between the theoretical and the experimental results. This means that the equation can be used to predict the final diameter of the grains obtained. This property is very

important to estimate the degree of hollowness of the grain and other physical properties like the mechanical properties and the flowability of a spray dried powder.

5 Conclusions

The drying behavior of silica nanofluid droplets was studied under different experimental condition. For this system, all the experiments tested presented first and second drying period. Moreover, a transition period could be observed depending of the interparticle forces present in the nanofluid. This transition period was longer and more significant in suspension electrostatically stabilized, where the capillary forces have to overcome the electrostatic repulsion.

Under the experimental conditions in which the drying tests were carried out, the crystallization of NaCl only on the grain surface showed that the evaporation front in those cases was located on the shell surface and not in its inner part. This means that evaporation of liquid took place at the surface of the grain.

The ANOVA analysis indicate that the air temperature, the initial droplet volume and the initial solid content were the input variables that have higher influence in the mass transfer rate for the first drying period. All of them present a positive effect meaning that an increase in their values leads to a faster drying. The increase in the gradient of temperature between the droplet surface and the surrounding air, and the increase of the mass transfer coefficient (due to the increase of Reynolds number) produce an increase in the heat and mass transfer between the droplet and the air.

Experimental drying curves were modeled using the REA model. Theoretical curves showed a good agreement with the experimental data. Correlations for the activation energy are shown for this system under different drying condition. Parameter a in the activation energy was found to be constant, parameter b was observed to depend on the solid content

and the air temperature, and finally, parameter *c* only depended on the solid content. Correlations for parameters *b* and *c* were obtained and used to predict drying curves providing good results. The volume of the droplet did not affect the activation energy equation but had an influence in the mass transfer coefficient.

Finally, from the drying curves, the critical moisture content and the final grain diameter could be predicted. The values obtained for the two grain properties showed good agreement with the experimental results.

Acknowledgments

R. Mondragón thanks the Spanish Ministry of Education for a pre-doctoral fellowship (FPU program, Ref. AP2008-01077).

Nomenclature

A	area [m^2]
d	droplet diameter [m]
D	diffusion coefficient [m^2/s]
h_m	mass transfer coefficient [m/s]
h_C	heat transfer coefficient [$J/(s \cdot m^2 \cdot K)$]
m	mass transfer rate [kg/s]
M	mass of component [kg]
R	gas constant [J/(mol·K)]
T	air temperature [ºC]
t	drying time [s]

V	volume [m^3]
X	dry basis moisture content [kg water/kg dry solid]
Y	mass fraction [kg component/kg suspension ≡ w/w]
y	droplet position [m]
ΔE_V	activation energy [J/mol]
ρ	density [kg/m^3]
φ	relative humidity [-]

Subscripts

a	air
cr	critical
d	droplet
eq	equilibrium
f	final
L	liquid
S	solid
sat	saturation
surf	surface
Sus	suspension
v	water vapor
0	initial

References

[1] Masters, K. Spray drying handbook; Longman Scientific and Technical, 1991.

[2] Kastner, O.; Brenn, G.; Rensink, D.; Tropea, C. The acoustic tube levitator: a novel device for determining the drying kinetics of single droplets. Chemical Engineering Technology 2001, 24, 335-339.

[3] Mezhericher, M.; Levy, A.; Borde, I. Theoretical models of single droplet drying kinetics: a review. Drying Technology 2010, 28, 278-293.

[4] Handscomb, C.S.; Kraft, M. Simulating the structural evolution of droplets following shell formation. Chemical Engineering Science 2010, 65, 713-725.

[5] Mezhericher, M.; Levy, A.; Borde, I. Modelling the morphological evolution of nanosuspension droplet in constant-rate drying stage. Chemical Engineering Science 2011, 66, 884-896.

[6] Ullum, T.; Sloth, J.; Brask, A.; Wahlberg, M. Predicting spray dryer deposits by CFD and an empirical drying model. Drying Technology 2010, 28, 723-729.

[7] Verdurmen, R.E.M.; Menn, P.; Ritzert, J.; Blei, S.; Nhumaio, G.C.S.; Sorensen, T.S.; Gunsing, M.; Straatsma, J.; Verschueren, M.; Sibeijn, M.; Schulte, G.; Fritsching, U.; Bauckhage, K.; Tropea, C.; Sommerfeld, M.; Watkins, A.P.; Yule, A.J.; Schonfeldt, H. Simulation of agglomeration in spray drying installations: The EDECAD project. Drying Technology 2004, 22, 1403-1461.

[8] Chen, X.D. The basics of a reaction engineering approach to modelling air-drying of small droplets or thin-layer materials. Drying Technology 2008, 26, 627-639.

[9] Chen, X.D.; Lin, S.X.Q. Air drying of milk droplet under constant and time-dependent conditions. AIChE Journal 2005, 51, 1790-1799.

[10] Chen, X.D.; Xie, G.Z. Fingerprints of the drying behavior of particulate or thin layer food materials established using a reaction engineering model. Food and Bioproduct Processes 1997, 75, 213-222.

[11] Elperin, T.; Krasovitov, B. Evaporation of liquid droplets containing small solid particles. International Journal of Heat and Mass Transfer 1995, 38, 2259–2267.

[12] Farid, M. A new approach to modelling of single droplet drying. Chemical Engineering Science 2003, 58, 2985-2993.

[13] Fyhr, C.; Kemp, I.C. Comparison of different drying kinetic models for single particles. Drying Technology 1998, 16, 1339-1369.

[14] Handscomb, C.S.; Kraft, M.; Bayly, A.E. A new model for the drying of droplets containing suspended solids after shell formation. Chemical Engineering Science 2009, 64, 228-246.

[15] Handscomb, C.S.; Kraft, M.; Bayly, A.E. A new model for the drying of droplets containing suspended solids. Chemical Engineering Science 2009, 64, 628-637.

[16] Mezhericher, M.; Levy, A.; Borde, I. Theoretical drying model of single droplets containing insoluble or dissolved solids. Drying Technology 2007, 25, 1035-1042.

[17] Mezhericher, M.; Levy, A.; Borde, I. Modelling of particles breakage during drying. Chemical Engineering and Processing 2008, 47, 1404-1411.

[18] Nesic, S.; Vodnik, J. Kinetics of droplet evaporation. Chemical Engineering Science 1991, 46, 527-537.

[19] Sano, Y.; Keey, R.B. The drying of a spherical particle containing colloidal material into a hollow sphere. Chemical Engineering Science 1982, 37, 881-889.

[20] Langrish, T.A.G.; Kockel, T.K. The assessment of a characteristic drying curve for milk powder for use in computational fluid dynamics modelling. Chemical Engineering Journal 2001, 84 69-74.

[21] Patel, K.C.; Chen, X.D. Prediction of spray-dried product quality using two simple drying kinetics models. Journal of Food Process Engineering 2005, 28, 567-594.

[22] Woo, M.W.; Wan Daud, W.R.; Mujumdar, A.S.; Meor Talib, M.Z.; Hua, W.Z.; Tasirin, S.M. Comparative study of droplet drying models for CFD modelling. Chemical Engineering Research and Design 2008, 86, 1038-1048.

[23] Fu, N.; Woo, M.W.; Lin, S.X.Q.; Zhou, Z.; Chen, X.D. Reaction engineering approach (REA) to model the drying kinetics of droplets with different initial sizes-experiments and analyses. Chemical Engineering Science 2011, 66, 1738-1747.

[24] Lin, S.X.Q.; Chen, X.D. A model for drying and aqueous lactose droplet using the reaction engineering approach. Drying Technology 2006, 24, 1329-1334.

[25] Lin, S.X.Q.; Chen, X.D. The reaction engineering approach to modelling cream and whey protein concentrate droplet drying. Chemical Engineering and Processing 2007, 46, 437-443.

[26] Patel, K.C.; Chen, X.D.; Lin, S.X.Q. A composite reaction engineering approach to drying of aqueous droplets containing sucrose, maltodextrin (DE6) and their mixtures. AIChE Journal 2009, 55, 217-231.

[27] Brenn, G. Concentration fields in evaporating droplets. International Journal of Heat and Mass Transfer 2005, 48, 395-402.

[28] Brenn, G.; Kastner, O.; Rensink, D.; Tropea, C. Evaporation and drying of multicomponent and multiphase droplets in a tube levitator. In Proceedings of the 15th

Annual Conference on Liquid Atomization and Spray Systems (ILASS Europe), Toulouse, 1999.

[29] Kastner, O.; Brenn, G.; Rensink, D.; Tropea, C.; Yarin, A.L. Investigation of the drying behavior of suspension droplets in an acoustic tube levitator. In Proceedings of the 16th Annual Conference on Liquid Atomization and Spray Systems (ILASS Europe), Darmstadt, 2000.

[30] Kastner, O.; Brenn, G.; Rensink, D.; Tropea, C. Mass transfer from multiphase droplets during drying in a tube levitator. In Proceedings of the 8th International Conference on Liquid Atomization and Spray Systems, Pasadena, 2000.

[31] Kastner, O.; Brenn, G.; Tropea, C. The drying time of single suspension droplets under various conditions. In Proceedings of Conference "Spray Drying and Related Processes", Dortmund, 2001.

[32] Mondragon, R.; Hernandez, L.; Julia, J.E.; Jarque, J.C.; Chiva, S.; Zaitone, B.; Tropea, C. Study of the drying behavior of high load multiphase droplets in an acoustic levitator at high temperature conditions. Chemical Engineering Science 2011, 66, 2734-2744.

[33] Mondragon, R.; Jarque, J.C.; Julia, J.E.; Hernandez, L.; Barba, A. Effect of slurry properties and operational conditions on the structure and properties of porcelain tile granules dried in an acoustic levitator. Journal of the European Ceramic Society 2012, 32, 59-70.

[34] Yarin, A.L.; Brenn, G.; Kastner, O.; Rensink, D.; Tropea, C. Evaporation of acoustically levitated droplets. Journal of Fluid Mechanics 1999, 399, 151-204.

[35] Yarin, A.L.; Weiss, D.A.; Brenn, G.; Rensink, D. Acoustically levitated drops: drop oscillation and break-up driven by ultrasound modulation. International Journal of Multiphase Flow 2002, 28, 887-910.

[36] Yarin, A.L.; Brenn, G.; Kastner, O.; Tropea, C. Drying of acoustically levitated droplets of liquid-solid suspensions: evaporation and crust formation. Physics of Fluids 2002, 14, 2289-2298.

[37] Zaitone, B.; Hunsmann, S.; Castanet, G.; Damaschke, N.; Ebert, V.; Tropea, C.. Evaporation of acoustically levitated droplets. In Proceedings of the 10th International Congress on Liquid Atomization and Spray Systems, Kyoto, 2006

[38] Omrane, A.; Santesson, S.; Alden, M.; Nilsson, S. Laser techniques in acoustically levitated micro droplets. Lab on a Chip - Miniaturisation for Chemistry and Biology 2004, 4, 287-291.

[39] Mondragon, R.; Julia, J.E.; Barba, A.; Jarque, J.C. Characterization of silica-water nanofluids dispersed with an ultrasound probe: a study of their physical properties and stability. Powder Technology 2012, 224, 138-146 .

[40] Hadinoto, K.; Cheow, W.S. Hollow spherical nanoparticulate aggregates as potential ultrasound contrast agent: shell thickness characterization. Drug Development and Industrial Pharmacy 2009, 35, 1169-1179.

[41] Walker, W.J.; Reed, J.S.; Verma, S.K. Influence of slurry parameters on the characteristics of spray-dried granules. Journal of the American Ceramic Society 1999, 82**,** 1711-1719.

[42] Bertrand, G. ; Filiatare, C.; Mahdjoub, H.; Foissy, A.; Coddet, C. Influence of slurry characteristics on the morphology of spray-dried alumina powders. Journal of the European Ceramic Society 2003, 23, 263-271.

[43] Sen, D.; Mazumder, S.; Melo, J.S.; Khan, A.; Bhattyacharya, S.; D'Souza, D.F. Evaporation driven self-assembly of a colloidal dispersion during spray drying: volume fraction dependent morphological transition. Langmuir 2009, 25, 6690-6695.

[44] Bahadur, J.; Sen, D.; Mazumder, S.; Paul, B.; Khan, A.; Ghosh, G. Evaporation-induced self assembly of nanoparticles in non-buckling regime: volume fraction dependent packing. Journal of Colloid and Interface Science 2010, 351, 357-364.

[45] Kawahara, N.; Yarin, A.L.; Brenn, G.; Kastner, O.; Durst, F. Effect of acoustic streaming on the mass transfer of a sublimating sphere. Physic of Fluids 2000, 12, 912-923.

[46] Ranz, W.E.; Marshall, J.R. Evaporation from drops 1. Chemical Engineering Progress 1952, 48, 141-146.

[47] Ranz, W.E.; Marshall, J.R. Evaporation from drops 2. Chemical Engineering Progress 1952, 48, 173-180.

[48] Zaitone, B.; Tropea, C. Evaporation of pure liquid droplets: Comparison of droplet evaporation in an acoustic field versus glass-filament. Chemical Engineering Science 2011, 66, 3914-3921.

Figure captions

Figure 1. Drying kinetic of a single droplet.

Figure 2. General sketch of the (a) experimental set-up and (b) acoustic levitator tube.

Figure 3. Evolution of the squared-diameter and the position of a silica nanofluid droplet in presence of (a) repulsive forces and (b) attractive forces.

Figure 4. Internal microstructure of the shell and salt crystallization at the surface: Ys=0.02, pH=2, $[NaCl]$=0.05 M (a) T=120ºC, V_0=0.8µl (b) T=80ºC, V_0=0.3µl.

Figure 5. Evolution of diameter for pure water droplets.

Figure 6. a) Standardized effects and b) main effects for the first period mass transfer rate.

Figure 7. Evolution of moisture content and droplet temperature for Ys=0.20, pH=2, $[NaCl]$=0 M, T=120ºC, V_0=0.8µl.

Figure 8. Drying curves: experimental data and REA model. (a) Ys=0.02, T=80ºC, (b) Ys=0.02, T=120ºC, (c) Ys=0.20, T=80ºC, (d) Ys=0.20, T=120ºC, (e) Ys=0.10, T=80ºC, (f) Ys=0.10, T=120ºC.

Figure 9. Drying curves: experimental data and REA model.

Figure 10. Critical moisture content determined experimentally and theoretically.

Figure 11. Final grain diameter determined experimentally and theoretically.

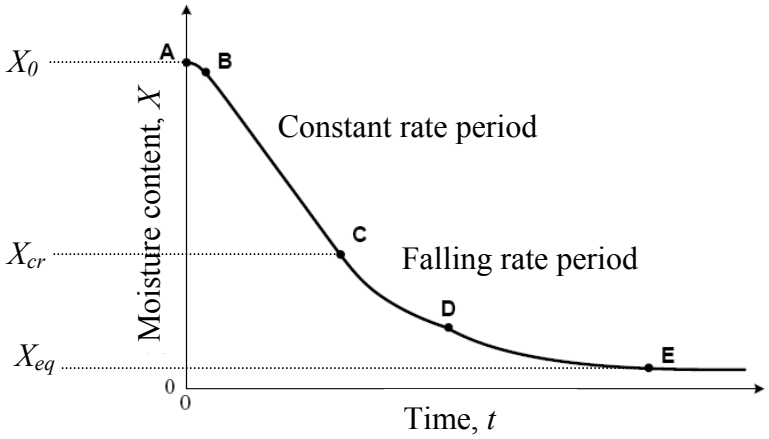

Figure 1. Drying kinetic of a single droplet.

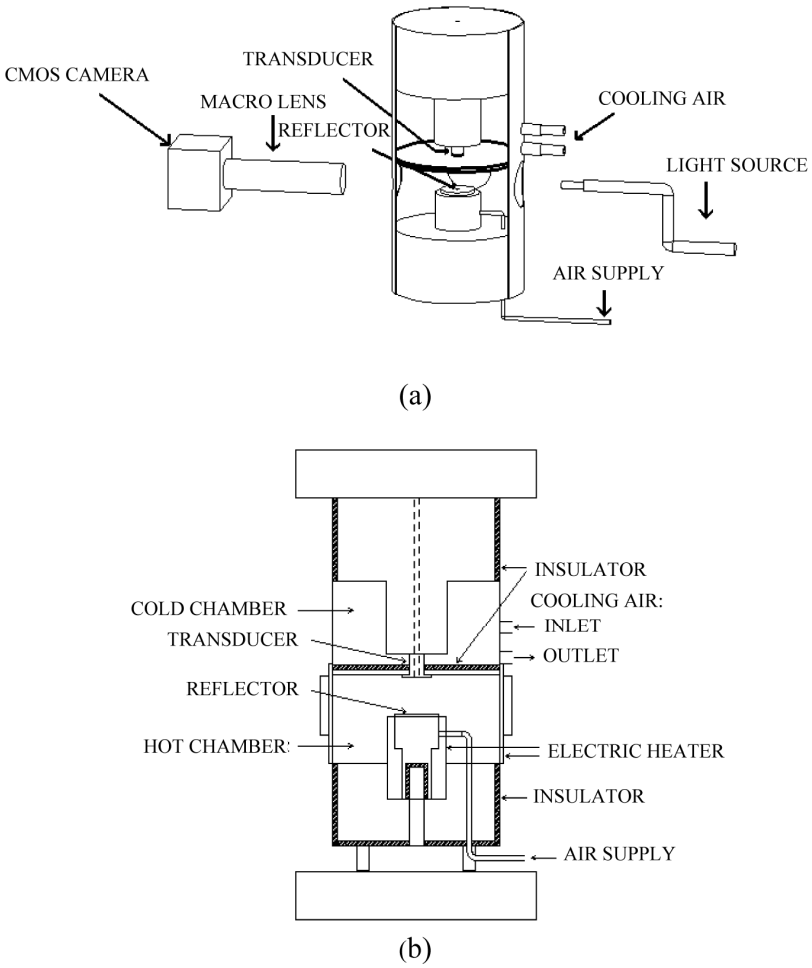

Figure 2. General sketch of the (a) experimental set-up and (b) acoustic levitator tube.

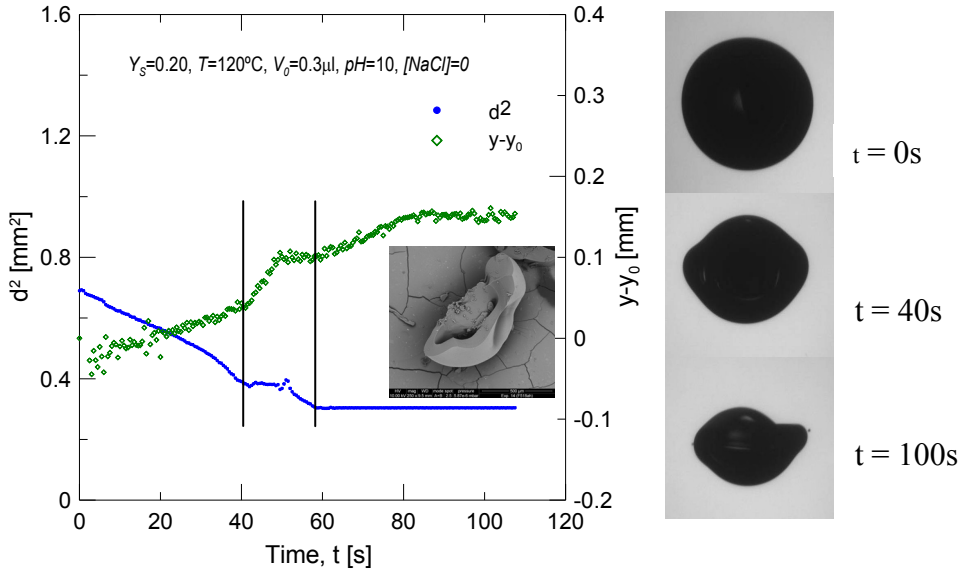

(a)

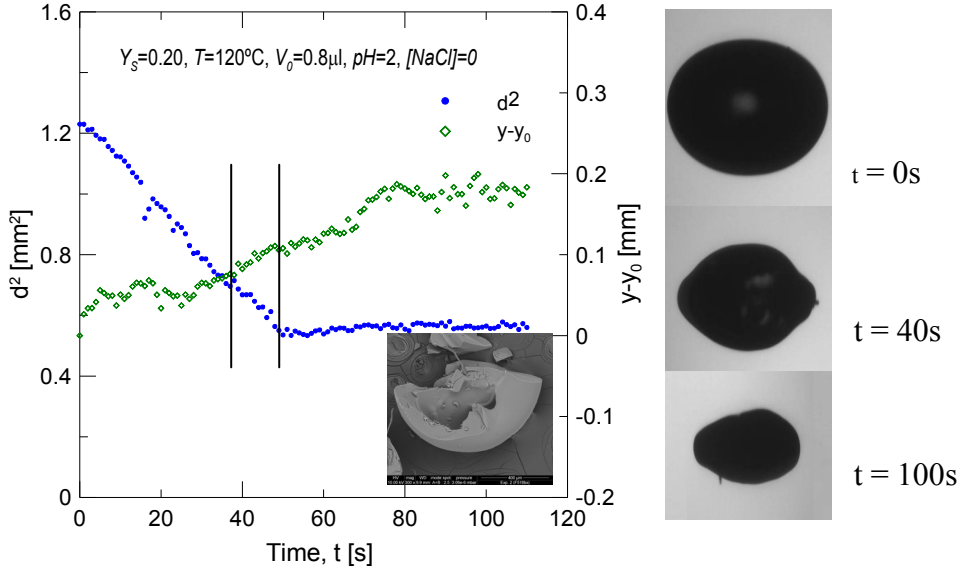

(b)

Figure 3. Evolution of the squared-diameter and the position of a silica nanofluid droplet in presence of (a) repulsive forces and (b) attractive forces.

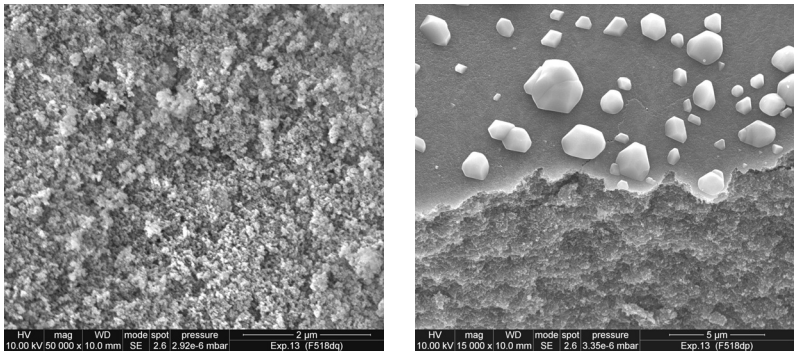

(a)

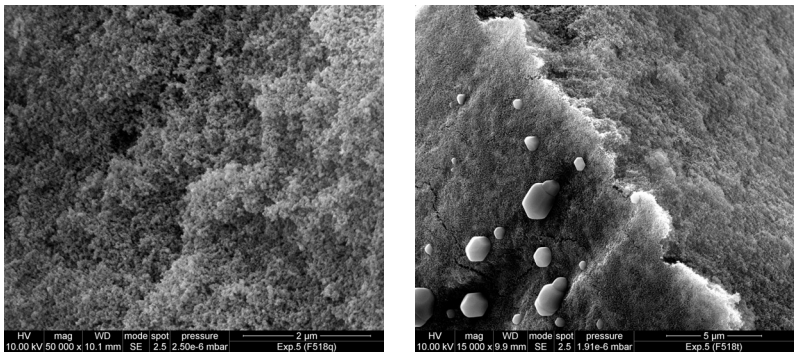

(b)

Figure 4. Internal microstructure of the shell and salt crystallization at the surface: *Ys*=0.02, *pH*=2, *[NaCl]*=0.05 M (a) *T*=120ºC, V_0=0.8µl (b) *T*=80ºC, V_0=0.3µl.

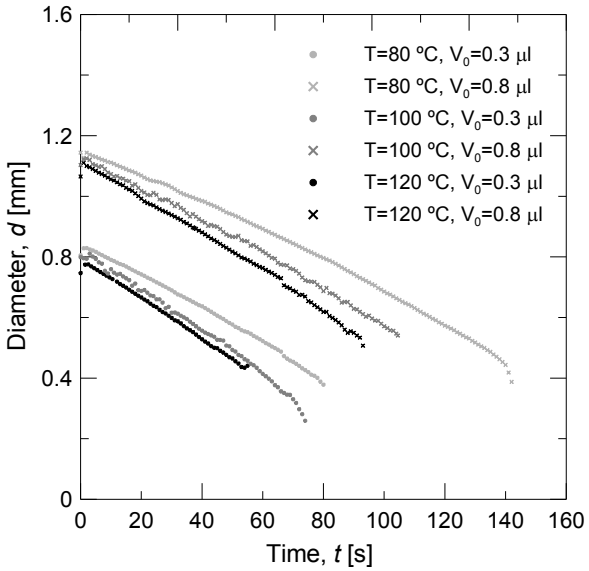

Figure 5. Evolution of diameter for pure water droplets.

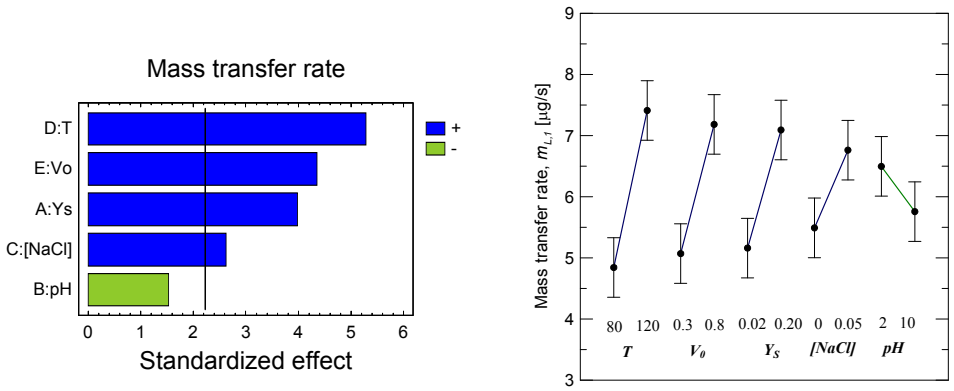

a) b)

Figure 6. a) Standardized effects and b) main effects for the first period mass transfer rate.

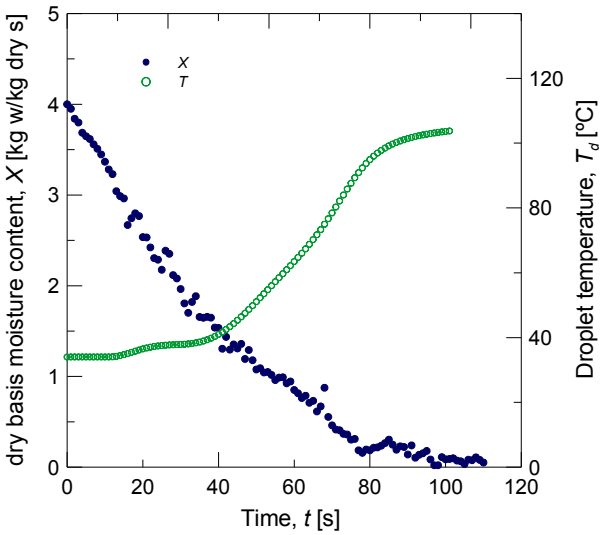

Figure 7. Evolution of moisture content and droplet temperature for *Ys*=0.20, *pH*=2, *[NaCl]*=0 M, *T*=120ºC, V_0=0.8µl.

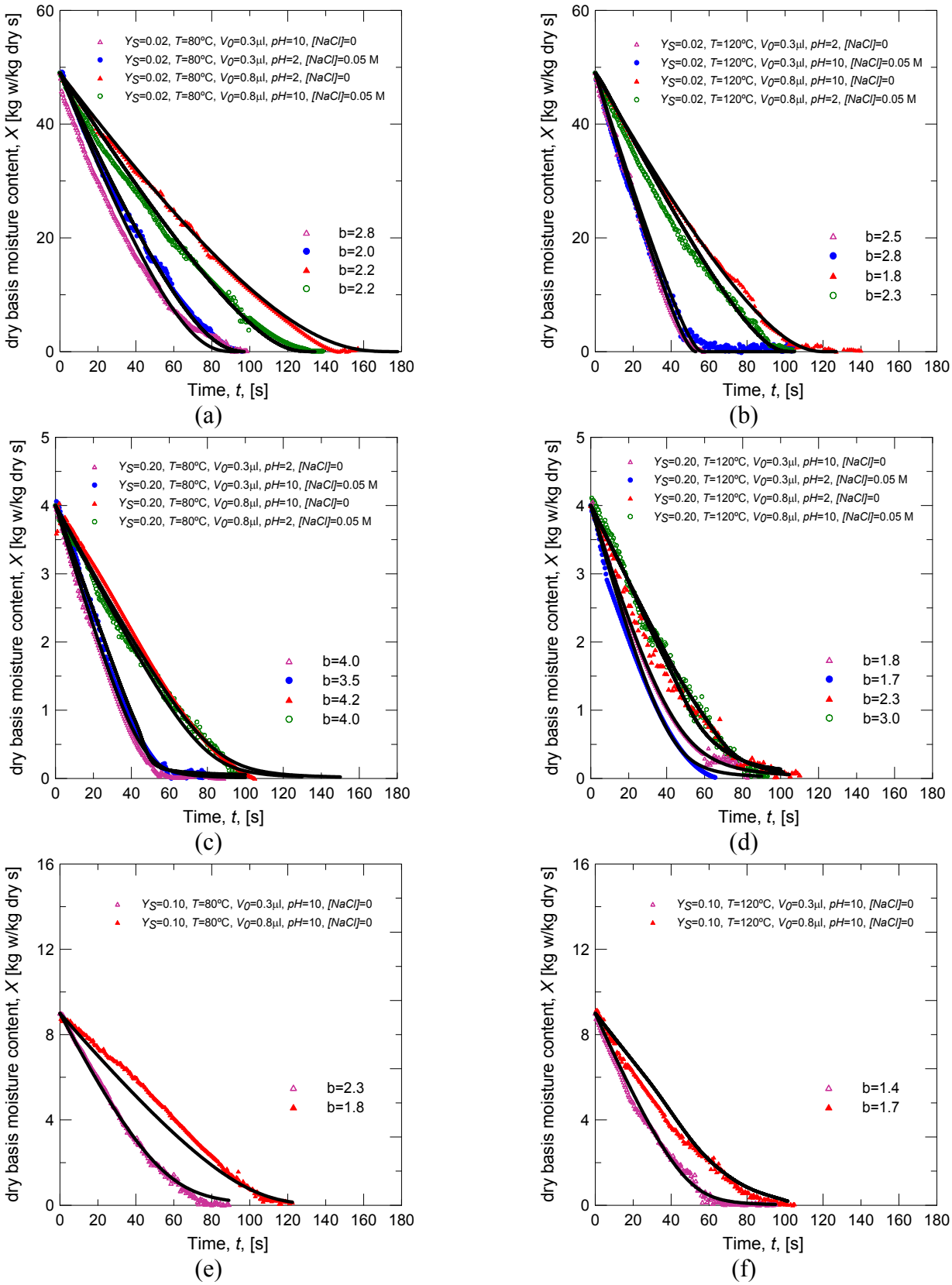

Figure 8. Drying curves: experimental data and REA model. (a) *Ys*=0.02, *T*=80ºC, (b) *Ys*=0.02, *T*=120ºC, (c) *Ys*=0.20, *T*=80ºC, (d) *Ys*=0.20, *T*=120ºC, (e) *Ys*=0.10, *T*=80ºC, (f) *Ys*=0.10, *T*=120ºC.

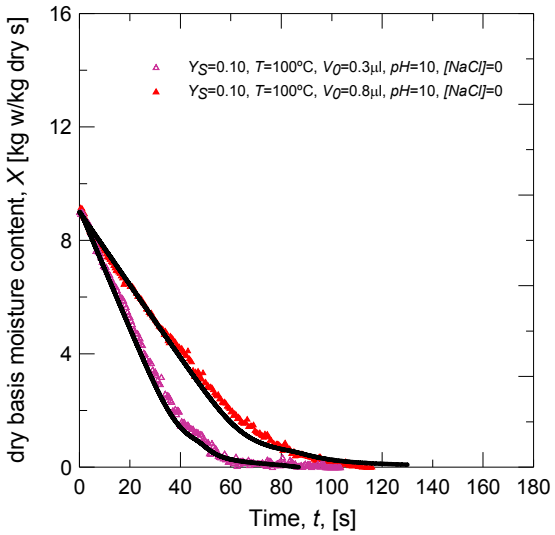

Figure 9. Drying curves: experimental data and REA model.

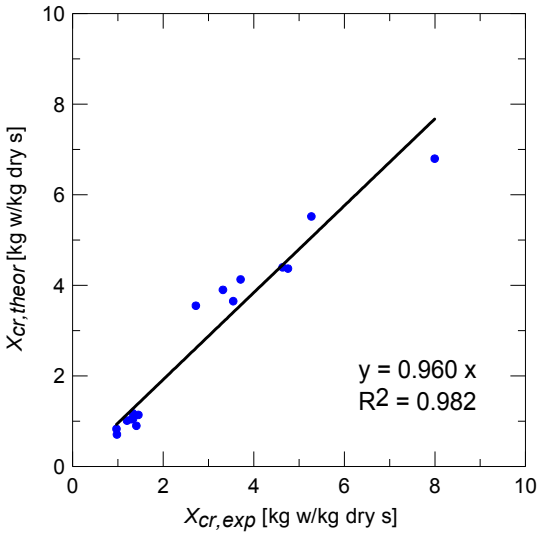

Figure 10. Critical moisture content determined experimentally and theoretically.

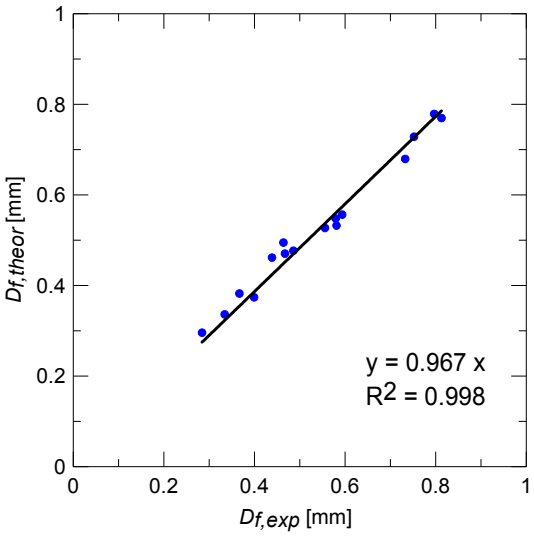

Figure 11. Final grain diameter determined experimentally and theoretically.

Table captions

Table 1. Mass transfer coefficients and Sherwood number**.**

Table 2. Activation energy coefficients.

Table 3. Activation energy coefficients for different materials.

Table 1. Mass transfer coefficients and Sherwood number.

Temperature, T, [°C]	Droplet volume, V_0, [μl]	h_m [m/s]	Sherwood, Sh (Eq. 12)	Sherwood, Sh (Eq. 7)
80	0.3	0.1094	3.48	5.26
	0.8	0.0857	3.58	5.78
100	0.3	0.0988	3.06	5.20
	0.8	0.0832	3.38	5.69
120	0.3	0.0798	2.42	5.16
	0.8	0.0796	3.16	5.65

Table 2. Activation energy coefficients.

Solid mass load, Y_S, [w/w]	Temperature, T, [ºC]	b	c	a
0.02	80 / 120	2.33	0.16	$3.15 \cdot 10^7$
0.10	80 / 120	2.20	0.69	
0.20	80	3.93	0.72	
	120	2.20		

Table 3. Activation energy coefficients for different materials.

Material	Drying conditions	Reference	*b*	*c*	*a*
Kiwifruit	T = 90 ºC Y_s = 0.13	Chen and Xie, 1997	1.00	1.02	$6.50 \cdot 10^5$
Milk	T = 65-107 ºC Y_s = 0.20-0.30	Chen and Lin, 2005	1.35	0.93	$2.43 \cdot 10^7$
Lactose	T = 80-100 ºC Y_s = 0.22	Lin and Chen., 2006	1.68	1.02	$2.25 \cdot 10^7$